RSC Advances

ROYAL SOCIETY OF CHEMISTRY

www.rsc.org/advances

Journal Name

RSCPublishing

ARTICLE

Synthesis of Cu_3P nanocubes and their excellent electrocatalytic efficiency for hydrogen evolution reaction in acidic solution

Cite this: DOI: 10.1039/x0xx00000x

Received 00th January 2012,
Accepted 00th January 2012

DOI: 10.1039/x0xx00000x

www.rsc.org/

Lianbo Ma,[a] Xiaoping Shen,*[a] Hu Zhou,[b] Jun Zhu,[a] Chunyan Xi,[a] Zhenyuan Ji [a] and Lirong Kong [a]

Cu_3P nanocubes are synthesized through a facile two-step strategy, which consists of a simple solution based method followed by a low-temperature phosphidation process. The Cu_3P nanocubes have an average size of about 198 nm, and show a three-dimensional (3D) cubic architecture with hollow interiors and thin cubic shells. The material as electrocatalyst for hydrogen evolution reaction (HER) is investigated in acidic solution. It is found that the Cu_3P nanocubes exhibit a low overpotential (145 mV), a small Tafel slope (70.2 mV per decade), and a large exchange current density (0.016 mA/cm^2). Moreover, the Cu_3P nanocubes show great electrochemical stability in acidic solution since no obvious decay in current density is observed after 1000 cycles. The excellent electrocatalytic performance can be associated with the electronic structures of Cu and P, as well as the hollow interior structure of Cu_3P nanocubes, which supplies more active sites for HER. The approach used here provides an effective route for synthesizing metal phosphides with various microstructures and functions.

Introduction

The ever increasing global demands for energy and the environmental pollution call for renewable and clean energy alternatives.[1] Hydrogen is considered to be such an ideal energy source due to its high energy density and zero environmental impact of the combustion products.[2,3] Despite the conventional ways for hydrogen production,[4,5] splitting of water by either electricity or light is considered to be the most promising way to produce hydrogen.[6,7] However, the production efficiency is low without the use of electrocatalysts, which can significantly reduce the large overpotential for hydrogen evolution reaction (HER).[8] To achieve the better efficiency, this key process usually demands the assistance of high-performance HER electrocatalysts. Take this into account, platinum (Pt) and Pt-group metals are the ideal electrocatalysts for HER because of their excellent electrocatalytic performance.[9,10] However, in spite of their high activity toward HER, the high cost and low abundance in earth severely restricted their large-scale application.[11] Therefore, the big challenge in hydrogen production is to reduce the use of noble metals or replace them with inexpensive non-precious metal catalysts.[12-14]

The mostly applied strategy to reduce the use of noble metals is to construct various unique nanostructures, and the nanostructures usually involve the exposure of more electroactive sites for HER. For instance, Bai *et al.* synthesized the electrocatalyst of PtPd nanocubes in which uniform thin Pt shells were attached on the Pd nanocubes, and the PtPd nanostructure exhibits an excellent electrocatalytic activity as HER catalyst.[15] On the other hand, exploring non-noble metals composites as HER catalysts is a promising way for hydrogen production.[16] Up to now, the most extensively investigated non-noble metals composites include metal alloys,[17,18] metal hydroxides,[19,20] chalcogenides,2[1,22] carbides,[23-25] nitrides,[26,27] as well as complexes.[28,29] These materials as electrocatalysts for HER exhibit remarkable electrocatalytic performance, and could be considered as the candidates for hydrogen production catalysts in practical application.

As a new type of electrocatalysts, metal phosphides, comprised of inexpensive and earth-abundant elements, have been reported to show high HER activity. The extensively investigated metals phosphides include FeP,[30,31] CoP,[32-36] Ni_2P,[37-40] WP[41], and MoP[42,43] *etc*. All of them show comparable electrocatalytic performances to noble metals catalysts. Recently, Tian *et al*. reported the self-supported Cu_3P nanowire arrays as a high-performance electrocatalyst for the generation of hydrogen from water, demonstrating that the Cu_3P material possesses a big possibility as HER catalyst.[44] Moreover, it is

already acknowledged that the morphology and nanostructure of the HER electrocatalyst affected the electrocatalytic efficiency significantly and the nanostructures with more electroactive sites favored the electrocatalytic performance.[45,46] Inspired by this, in this work, we fabricated the Cu_3P nanocubes with a hollow interior nanostructure through a simple solution based method followed by a low-temperature phosphidation process. The as-prepared Cu_3P nanocube exhibits excellent catalytic activity for HER, indicating its promising application as electrocatalyst for practical hydrogen production.

Experimental

Chemicals and synthesis of the Cu_3P nanocubes

All Chemicals in this work are of analytical purity and used without further purification. In a typical synthesis, 1.0 mmol of $CuCl_2 \cdot 2H_2O$ was dissolved in 100 mL of deionized water under vigorous stirring. Then, 10 mL of NaOH aqueous solution (2.0 mol L^{-1}) was added into the above mixture under stirring in water bath at 40 °C. After stirring for 30 min, 10 mL of ascorbic acid solution (0.6 mol L^{-1}) was introduced into the dark brown solution, and then a red liquid was formed gradually. Finally, the mixture was further aged for 3 h. The sediments were then collected by centrifugation, washed with deionized water for several times and dried in an oven at 45 °C. In order to get the final product, 20 mg of the as-obtained sample and 120 mg of sodium hypophosphite (NaH_2PO_2) were mixed together and ground to a fine powder by using a mortar. The mixture was then thermally annealed in N_2 atmosphere at 300 °C for 2 h with a heating rate of 3 °C/min. After the system was cooled down to room temperature naturally, the as-obtained powder was washed with deionized water for several times, dried at 45 °C for 24 h, and then collected for characterization.

Instrumentation and measurements

The phase structure of the as-synthesized samples were characterized by power X-ray diffraction (XRD) on a Bruker D-8 Advance diffractometer using Cu Kα (λ = 1.5406 Å) radiation. The morphology, microstructure and size of the products were examined by field emitting scanning electron microscopy (FESEM, JSM-6480) and transmission electron microscopy (TEM, JEM-2100). The composition of the product was determined by energy-dispersive X-ray spectrometry (EDS). The EDS was recorded with an energy dispersive spectrometer attached to a scanning electron microscopy (JSM-6480).

Electrocatalytic activity for HER

The catalytic activities of the as-prepared composites toward HER were conducted on a typical three-electrode setup using a CHI 760 D electrochemical analyzer (Chen Hua Instruments, Shanghai China) at room temperature. Saturated calomel electrode (SCE) and Pt foil were used as the reference and counter electrodes, respectively. Glassy carbon electrode (GCE, 3 mm in diameter) coated with the as-prepared composites (Cu_2O or Cu_3P nanocubes) were used as the working electrodes. As references, the electrochemical performances of commercial Pt/C and bare GCE were also conducted. Prior to the surface coating, the GCE was polished using 0.05 μm alumina powder, followed by ultrasonication in absolute ethanol, and then allowed to dry at room temperature. For the fabrication of working electrode, catalyst ink was prepared by dispersing 5 mg of catalyst into a mixed solvent containing 0.96 mL of absolute ethanol and 40 μL of 5 wt% Nafion solution, and then the mixture was ultrasonicated for about 30 min to form a homogeneous ink. Then 4 μL of the catalyst ink was loaded onto GCE and dried at room temperature naturally. Linear sweep voltammetry (LSV) was conducted at the scan rate of 2 mV s^{-1} with an electrolyte solution of 0.5 M H_2SO_4. All the potentials reported in our work were calibrated with the reversible hydrogen electrode (RHE). The potential was converted to the RHE electrode according to the equation: E (RHE) = E (SCE) + 0.281 V.

Results and discussion

Synthesis of the Cu_3P nanocubes

In this work, we synthesized the Cu_3P nanocubes through a facile two-step strategy, which consists of a solution based procedure and a low-temperature thermal annealing process. The involved reaction can be expressed as follows:

$$Cu^{2+} + 2OH^- = Cu(OH)_2 \quad (1)$$

$$2Cu(OH)_2 + C_6H_8O_6 = Cu_2O + C_6H_6O_6 + 3H_2O \quad (2)$$

$$2NaH_2PO_2 = PH_3\uparrow + Na_2HPO_4 \quad (3)$$

$$2PH_3 + 3Cu_2O = 2Cu_3P + 3H_2O \quad (4)$$

Firstly, $Cu(OH)_2$ was synthesized in the alkaline solution (reaction 1). It is acknowledged that ascorbic acid could act as mild reducing agent for the reduction of metal ions,[47,48] and it is also crucial for the formation of cubic microstructures of the products.[49] When the ascorbic acid was added into the reaction mixture, $Cu(OH)_2$ was converted to Cu_2O nanocubes *via* a redox reaction (reaction 2). Then the Cu_3P nanocubes were formed through a low-temperature phosphidation process. The conversion of Cu_2O into Cu_3P could be explained as follows: the Cu_2O was reduced to Cu element by PH_3,[50] which was generated *in situ* from the thermal decomposed NaH_2PO_4 (reaction 3), and then the resulting Cu subsequently catalyzes the decomposition of PH_3 into elemental P. Finally, the elemental P further reacts with Cu to form Cu_3P nanocubes (reaction 4).[51]

Characterization of the Cu_3P nanocubes

The phase structures of the products were firstly determined by XRD diffraction. Fig. 1 shows the XRD patterns of the Cu_2O and Cu_3P nanocubes. The observed diffraction peaks at 2θ values of 29.7°, 36.5°, 42.4°, and 61.6° can be ascribed to the (110), (111), (200), and (220) planes of the cubic Cu_2O (JCPDS No. 77-0199), indicating the successful preparation of the Cu_2O

in the first step. After the phosphidation process, several conspicuous diffraction peaks were detected at 2θ values of 28.5°, 36.0°, 39.1°, 41.6°, 45.1°, 46.2°, 47.3°, 53.5°, 59.9°, and 66.5°, which can be identified as the (111), (112), (202), (211), (300), (113), (212), (104), (222), and (223) planes of the cubic Cu_3P (JCPDS No. 71-2261), suggesting the formation of the Cu_3P nanocubes in the thermal annealing process. The survey spectra of X-ray photoelectron spectroscopy (XPS) for both Cu_2O and Cu_3P nanocubes are provided in Fig. S1, further suggesting the formation of these materials. The EDS spectrum of the Cu_3P nanocubes was presented in Fig. S2 (see Supporting Information), the Cu and P elements were detected. The atomic ratio of Cu to P was found to be almost 3 : 1, which is well consistent with that of Cu_3P.

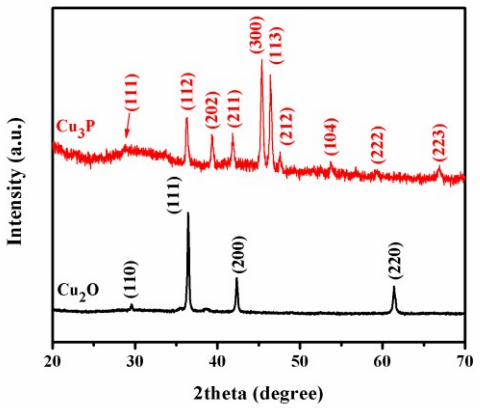

Fig. 1 XRD patterns of Cu_2O and Cu_3P products.

The morphology of the as-prepared samples was then examined by FESEM, TEM and high-resolution TEM (HRTEM). The typical low-magnification FESEM image of the Cu_2O is presented in Fig. 2a, which clearly illustrates that the Cu_2O is composed of many well-defined nanoboxes. Fig. 2b shows the TEM image of the Cu_2O product. Cubic morphology can be seen for each particle, which is well consistent with the SEM observation. The TEM image (Fig. 2b) reveals that the average size of the cubes is about 208 nm (Fig. S3a, see Supporting Information). Fig. 2c shows the magnified view of a typical nanocube, rough surfaces can be observed. The HRTEM image of the Cu_2O sample is presented in Fig. 2d, the as-observed interplanar spacings of 0.24 and 0.21 nm match well with the (111) and (200) lattice planes of the cubic Cu_2O, respectively, further confirming the successful preparation of Cu_2O nanocubes in the first step.

After phosphidation, the morphology of product was investigated, and the results are shown in Fig. 3. The FESEM image (Fig. 3a) reveals that the product can basically maintains the cubic nanostructures after the phosphidation process. The detailed morphology was further investigated by TEM technique. Cubic nanostructure with an average size of about 198 nm (Fig. S3b, see Supporting Information) is observed in Fig. 3b, which is smaller than that of Cu_2O. This can be ascribed to the shrinkage of the nanocubes in the thermal annealing process. In the TEM image with higher magnification (Fig. 3c), the interior part shows a lower contrast, indicating a

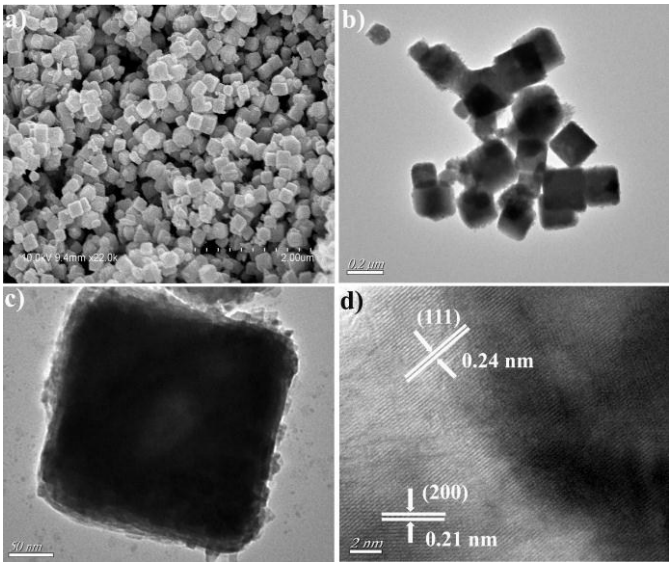

Fig. 2 (a) FESEM, (b, c) TEM and (d) HRTEM images of the Cu_2O product.

hollow interior and architecture. The HRTEM image (Fig. 3d) further reveals the successful preparation of Cu_3P, the interplanar spacing of 0.25 nm agrees well with the (112) lattice plane of Cu_3P. The EDX elemental mapping (Fig. S4) further demonstrated the homogeneous distribution of Cu and P elements in the Cu_3P nanocube. These results demonstrate that the approach used is an effective strategy for the synthesis of metal phosphides.

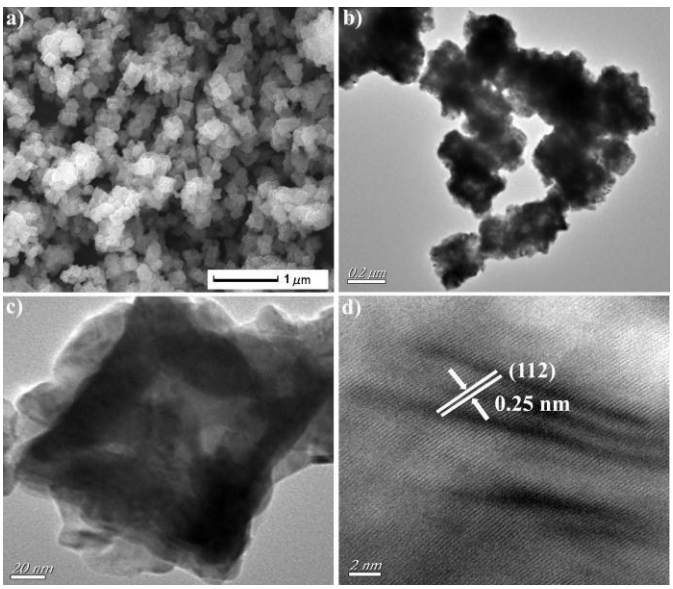

Fig. 3 (a) FESEM, (b, c) TEM and (d) HRTEM images of Cu_3P product.

Electrocatalytic activity toward HER

To evaluate the electrocatalytic activity of the as-prepared products, the Cu_2O and Cu_3P nanocubes were deposited on GCEs with a loading amount of 0.29 mg/cm^2. Before the LSV measurements, CV was performed to stabilize or saturate the electrocatalysts in the electrolyte, the results of which are shown in Fig. S5 (see Supporting Information). Fig. 4 shows the LSV polarization curve of Cu_3P nanocubes and Cu_2O electrodes in 0.5 M H_2SO_4 solution with a scan rate of 2 mV s^{-1}. As control experiments, the electrochemical performances of commercial Pt/C electrode and bare GCE were also investigated for comparison. Obviously, the Pt/C electrode shows the lowest overpotential, indicating the highest electrocatalytic activity for HER, while the bare GCE electrode shows no electroactivity within the overpotential range of 0-0.60 V *vs*. RHE.[52] The Cu_2O nanocubes show poor electrocatalytic activity with an onset overpotential value of 385 mV. In sharp contrast, Cu_3P nanocube is significantly active for HER with an onset overpotential as low as 145 mV, and the additional negative potential leads to rapid rise of the cathodic current. This result may be attributed to the special composition and unique structure of Cu_3P nanocubes. On one hand, the Cu_3P material shows distinct electronic structure induced by the presence of non-metal elements in the metal lattice.[53] Both the Cu center (δ^+) and the proximal pendant base P (δ^-) are believed to be responsible for the hydrogen generation.[34] On the other hand, the Cu_3P nanocubes show a hollow interior and three-dimensional (3D) architecture with thin cubic shell structures, which can provide more active sites for the HER. More active sites favor the effective contact with the electrolyte ions, and thus improve the electrocatalytic efficiency for HER.[54,55] In addition, a high current density of 94.5 mA/cm^2 is obtained at the overpotential of 0.60 V, further suggesting the high electrocatalytic efficiency of the Cu_3P nanocubes. Fig. S6 (see Supporting Information) shows the optical photograph of the Cu_3P nanocubes on GCE during a LSV scan, indicating the production of many hydrogen bubbles on the electrode surface. These results demonstrate the promising application of Cu_3P nanocubes as a good electrocatalyst candidate for HER.

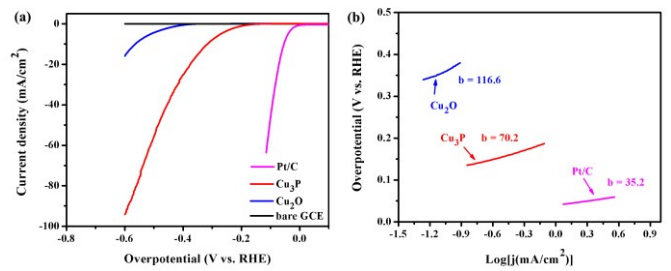

Fig. 4 (a) LSV polarization curves of Cu_3P, Cu_2O, Pt/C and bare GCE electrodes, (b) the corresponding Tafel slopes of Cu_3P, Cu_2O and Pt/C electrodes.

Based on the LSV polarization curves of Cu_3P, Cu_2O and Pt/C electrodes, the corresponding Tafel slopes were calculated, and the results are presented in Fig. 4b. The Tafel plots fit well to the Tafel equation ($\eta = b\log j + a$, where j is the current density and b is the Tafel slope), and the detailed parameters about the HER are calculated. It can be seen that the Tafel slope for Cu_3P nanocubes is 70.2 mV per decade, much lower than that of Cu_2O nanocubes (116.6 mV per decade) and those of other related HER catalysts.[54,56-58] These results indicate that the Cu_3P nanocubes possess high electrocatalytic efficiency. However, compared with that of Pt/C electrocatalyst (35.2 mV per decade), the electrocatalytic activity of Cu_3P electrocatalysts is still relatively low. According to the classical two-electron-reaction model, the Tafel slope is an inherent property of the catalyst which is determined by the rate-limiting step of the HER.[56] Three possible principle steps have been proposed for the HER in acidic medium. The first is a primary discharge step (Volmer reaction): $H_3O^+ + e^- \rightarrow H_{ads} + H_2O$, which is followed by either the electrochemical desorption step (Heyrovsky reaction): $H_{ads} + H_3O^+ + e^- \rightarrow H_2 + H_2O$, or the recombination step (Tafel reaction): $H_{ads} + H_{ads} \rightarrow H_2$. The rate determining step in the HER process can be assigned to a Volmer, Heyrovsky, or Tafel reaction by a Tafel slope of 116, 38, 29 mV per decade.[59] The experimental Tafel slope of the Cu_3P nanocubes (70.2 mV per decade) suggests that the HER on the surface of the Cu_3P nanocubes might follow a Volmer-Heyrovsky mechanism,[16,60,61] and the rates of the discharge step and the desorption step might be comparable during the HER process.[21] The exchange current density is usually expressed in terms of projected or geometric surface area and depends on the surface roughness. The capacitances (Fig. S7) for Cu_2O and Cu_3P are *ca*. 3.84 and 10.8 mF/cm^2, respectively, further suggesting that the Cu_3P electrode possesses much higher number of exposed active sites.

As an important parameter, the exchange current density (j_0) is usually used to estimate the electrocatalytic activity for HER. The high j_0 value indicates that the catalyst has good electrocatalytic efficiency.[62] The j_0 value for the Cu_3P nanocube is 0.016 mA/cm^2, 3.0 times higher than that of Cu_2O catalyst (0.004 mA/cm^2). Although the Cu_3P catalyst here exhibits a slightly lower catalytic activity as compared with some of other reported transition metal phosphides,[30-45] it supplies a promising candidate for HER catalysts.

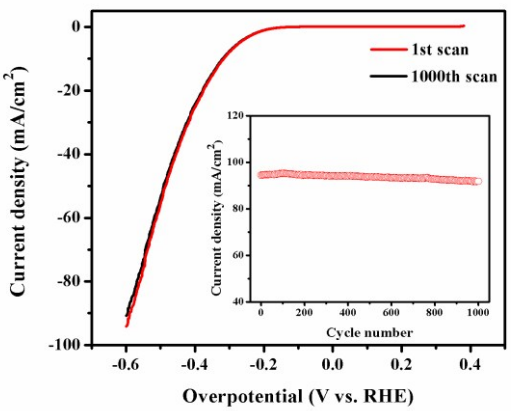

Fig. 5 The LSV polarization curves of the Cu_3P electrode at the 1st and the 1000th cycle number. The inset shows the current density of the Cu_3P electrode as a function of scan number at η = 0.6 V.

The long-term stability of an electrode is another important issue to consider for practical applications. The electrochemical stability of the Cu_3P nanocubes was assessed by repeating the LSV polarization scan for 1000 times, and the results are shown in Fig. 5. Only a tiny decay of the current density, from 94.5 to 91.8 mA/cm^2 at η = 0.6 V, is observed after 1000 cycles. This suggests that a high catalytic efficiency of the Cu_3P catalyst can be maintained after a long periodic scan time. The inset of Fig. 5 presents the current densities for Cu_3P nanocubes at various LSV scan number. It can be seen that the current density increases a little in the first 100 cycles, and then it remains stable in the residual cycles, indicating the high electrochemical stability of the Cu_3P nanocube catalyst for HER in acidic solution. For comparison, the electrocatalytic stability of the Cu_2O product was also investigated, as shown in Fig. S8 (see Supporting Information), a significant decay in current density is observed after 500 cycles. Further compared with other reported HER catalysts,[30,39,40] our Cu_3P nanocube catalyst also exhibits better cyclic performance, indicating that the Cu_3P nanocubes promise great application in practical hydrogen production in acidic medium.

Conclusions

In summary, Cu_3P nanocubes with an average size of about 198 nm are fabricated through a facile two-step strategy, which consists of a simple solution reaction and a low-temperature phosphidation process. The as-prepared Cu_3P material as HER electrocatalyst displays excellent catalytic performance for electrochemical hydrogen generation. Specially, the Cu_3P nanocubes exhibit a low onset overpotential (145 mV), a small Tafel slope (70.2 mV per decade), and a high exchange current density (0.016 mA/cm^2). Moreover, the Cu_3P nanocubes show high electrochemical stability in acidic solution. The excellent electrocatalytic efficiency of the Cu_3P catalyst for HER can be attributed to the electronic structures of Cu and P, as well as its unique microstructure. The approach used here provides an effective route for synthesizing other metal phosphides with various unique nanostructures, and the high electrocatalytic performance of Cu_3P nanocubes would find applications in practical hydrogen production.

Acknowledgements

The authors are grateful for financial support from National Nature Science Foundation of China (No. 51272094, 51072071) and Specialized Research Funds for the Doctoral Program of Higher Education of China (No. 20123227110018), China Postdoctoral Science Foundation (2014M561578) and Jiangsu Planned Projects for Postdoctoral Research Funds (1401109C).

Notes and references

[a] School of Chemistry and Chemical Engineering, Jiangsu University, Zhenjiang 212013, P. R. China, Fax: (+86)511-88791800; Tel: (+86)511-88791800; E-mail: xiaopingshen@163.com
[b] School of Material Science and Engineering, Jiangsu University, Zhenjiang 212003, P. R. China

1 J. A. Turner, *Science*, 2004, **305**, 972−974.
2 T. R. Cook, D. K. Dogutan, S. Y. Reece, Y. Surendranath, T. S. Teets and D. G. Nocera, *Chem. Rev.*, 2010, **110**, 6474−6502.
3 A. I. Hochbaum and P. Yang, *Chem. Rev.*, 2010, **110**, 527−546.
4 M. A. Rosen and D. S. Scott, *Int. J. Hydrogen Energy*, 1998, **23**, 653−659.
5 D. Trommer, F. Noembrini, A. Fasciana, D. Rodriguez, A. Morales, M. Romero and A. Steinfeid, *Int. J. Hydrogen Energy*, 2005, **30**, 605−618.
6 A. Midilli and I. Dincer, *Int. J. Hydrogen Energy*, 2007, **32**, 511−524.
7 M. G. Walter, E. L. Warren, J. R. McKone, S. W. Boettcher, Q. X. Mi, E. A. Santori and N. S. Lewis, *Chem. Rev.*, 2010, **110**, 6446−6473.
8 Z.Y. Lu, H.C. Zhang, W. Zhu, X.Y. Yu, Y. Kuang, Z. Chang, X.D. Lei, X.M. Sun, Chem. Commun., 2013, 49(68), 7516−7518.
9 H. B. Gray, *Nat. Chem.*, 2009, **1**, 112−112.
10 D. Merki and X. Hu, *Energy Environ. Sci.*, 2011, **4**, 3878−3888.
11 J. Greeley, T. F. Jaramillo, J. Bonde, I. Chorkendorff and J. K. Norskov, *Nat. Mater.*, 2006, **5**, 909−913.
12 D. V. Esposito, S. T. Hunt, Y. C. Kimmel and J. G. Chen, *J. Am. Chem. Soc.*, 2012, **134**, 3025−3033.
13 X. Wang, K. Maeda, A. Thomas, K. Takanabe, G. Xin, J. M. Carlsson, K. Domen and M. Antonietti, *Nat. Mater.*, 2009, **8**, 76−80.
14 S. Cobo, J. Heidkamp, P. A. Jacques, J. Fize, V. Fourmond, L. Guetaz, B. Jousselme, V. Ivanova, H. Dau, S. Palacin, M. Fontecave and V. Artero, *Nat. Mater.*, 2012, **11**, 802−807.
15 S. Bai, C. Wang, M. Deng, M. Gong, Y. Bai, J. Jiang and Y. J. Xiong, *Angew. Chem. Int. Ed.*, 2014, **53**, 12120−12124.
16 W. F. Chen, S. lyer, S, lyer, K. Sasaki, C. H. Wang, Y. M. Zhu, J. T. Mucherman and E. Fujita, *Energy Environ. Sci.*, 2013, **6**, 1818−1826.
17 Q. Yuan, Z. Y. Zhou, J. Zhuang and X. Wang, *Chem. Commun.*, 2010, **46**, 1491−1493.
18 M. K. Min, J. H. Cho, K. W. Cho, H. Kim, *Electrochim. Acta*, 2000, **45**, 4211−4217.
19 S. Fukuzumi and Y. Yamada, *J. Mater. Chem.*, 2012, **22**, 24284-24296.
20 S. Baranton and C. Coutanceau, *Appl. Catal. B*, 2013, **136**, 1−8.
21 M. R. Gao, Z. Y. Lin, T. T. Zhuang, J. Jiang, Y. F. Xu, Y. R. Zheng and S. H. Yu, *J. Mater. Chem.*, 2012, **22**, 13662−13668.
22 H. Tang, K. P. Dou, C. C. Kaun, Q. Kuang and S. H. Yang, *J. Mater. Chem. A*, 2014, **2**, 360−364.
23 F. Harnisch, G. Sievers, U. Schroder, *Appl. Catal. B*, 2009, **89**, 455−458.
24 Y. Liu, T. G. Kelly, J. G. G. Chen and W. E. Mustain, *ACS Catal.*, 2013, **3**, 1184−1194.
25 D. V. Esposito, S. T. Hunt, A. L. Stottlemyer, K. D. Dobson, B. E. McCandless, R. W. Birkmire and J. G. G. Chen, *Angew. Chem. Int. Ed.*, 2010, **49**, 9859−9862.
26 D. Choi and P. N. Kumta, *J. Am. Ceram. Soc.*, 2007, **90**, 3113−3120.
27 W. Zheng, T. P. Cotter, P. Kaghazchi, T. Jacob, B. Frank, K. Schlichte, W. Zhang, D. S. Su, F. Schu¨th and R. Schlogl, *J. Am. Chem. Soc.*, 2013, **135**, 3458−3464.

28 W. F. Chen, K. Sasaki, C. Ma, A. I. Frenkel, N. Marinkovic, J. T. Muckerman, Y. M. Zhu, R. R. Adzic, *Angew. Chem. Int. Ed.*, 2012, **51**, 6131−6135.
29 W. J. Zhou, X. J. Wu, X. H. Cao, X. Huang, C. L. Tan, J. Tian, H. Liu, J. Y. Wang and H. Zhang, *Energy Environ. Sci.*, 2013, **6**, 2921−2924.
30 Y. Xu, R. Wu, J. F. Zhang, Y. M. Shi and B. Zhang, *Chem. Commun.*, 2013, **49**, 6656-6658.
31 Y. Liang, Q. Liu, A. M. Asiri, X. P. Sun, Y. L. Luo, *ACS Catal.*, 2014, **4**, 4065−4069.
32 J. F. Chang, Y. Xiao, M. L. Xiao, J. J. Ge, C. P. Liu, W. Xing, *ACS Catal.*, 2015, **5**, 6874−6878.
33 J. Tian, Q. Liu, A. M. Asiri, X. P. Sun, *J. Am. Chem. Soc*., 2014, **136**, 7587−7590.
34 Z. Pu, Q. Liu, P. Jiang, A. M. Asiri, A. Y. Obaid, X. P. Sun, *Chem. Mater*., 2014, **26**, 4326−4329.
35 J. F. Callejas, C. G. Read, E. J. Popczun, J. M. Mcenaney, R. E. Schaak, *Chem. Mater*., 2015, **27**, 3769−3774.
36 E. J. Popczun, C. G. Read, C. W. Roske, N. S. Lewis and R. E. Schaak, *Angew. Chem. Int. Ed.*, 2014, **126**, 5531−5534.
37 X. G. Wang, Y. V. Kolenko, X. Q. Bao, K. Kovnir, L. F. Liu, *Angew. Chem. Int. Ed.*, 2015, **54**, 8188-8192.
38 Z. Pu, Q. Liu, C. Tang, A. M. Asiri, X. P. Sun, *Nanoscale*, 2014, **6**, 11031-11034.
39 P. Liu, J. A. Rodriguez, T. Asakura, J. O. Gomes and K. Nakamura, *J. Phys. Chem. B*, 2005, **109**, 4575−4583.
40 S. T. Oyama, *J. Catal*., 2003, **216**, 343-352.
41 Z. H. Pu, Q. Liu, A. M. Asiri, X. P. Sun, *ACS Appl. Mater. Interfaces*, 2014, **6**, 21874−21879.
42 X. B. Chen, D. Z. Wang, Z. P. Wang, P. Zhou, Z. Z. Wu and F. Jiang, *Chem. Commun.*, 2014, **50**, 11683−11685.
43 W. Cui, Q. Liu, Z. C. Xing, A. M. Asiri, K. A. Alamry and X. P. Sun, *Appl. Catal. B*, 2015, **164**, 144−150.
44 J. Q. Tian, Q. Liu, N. Y. Cheng, A. M. Asiri and X. P. Sun, *Angew. Chem. Int. Ed.*, 2014, **53**, 9577-9581.
45 Q. Liu, J. Q. Tian, W. Cui, P. Jiang, N. Y. Cheng, A. M. Asiri and X. P. Sun, *Angew. Chem. Int. Ed.*, 2014, **53**, 6710−6714.
46 L. Liao, J. Zhu, X. Bian, L. Zhu, M. D. Scanlon, H. H. Girault and B. Liu, *Adv. Funct. Mater*., 2013, **23**, 5326−5333.
47 S. W. Kang, Y. W. Lee, Y. S. Park, B. S. Choi, J. W. Hong, K. H. Park and S. W. Han, *ACS Nano*, 2013, **7**, 7945−7955.
48 P. Zhang, Y. H. Ma, Z. Y. Zhang, X. He, J. Zhang, Z. Guo, R. Z. Tai, Y. L. Zhao and Z. F. Chai, *ACS Nano*, 2012, **6**, 9943−9950.
49 Y. Fu, J. M. Song, Y. Q. Zhu and C. B. Cao, *J. Power Sources*, 2014, **262**, 344−348.
50 Q. Guan and W. Li, *J. Catal.*, 2010, **271**, 413−415.
51 A. E. Henkes, Y. Vasquez and R. E. Schaak, *J. Am. Chem. Soc*., 2007, **129**, 1896−1897.
52 D. Y. Chung, S. K. Park, Y. H. Chung, S. H. Yu, D. H. Lim, N. Jung, H. C. Ham, H. Y. Park, Y. Z. Piao, S. J. Yoo and Y. E. Sung, *Nanoscale*, 2014, **6**, 2131−2136.
53 P. Liu and J. A. Rodriguez, *J. Am. Chem. Soc*., 2005, **127**, 14871–14878.
54 C. B. Ma, X. Y. Qi, B. Chen, S. Y. Bao, Z. Y. Yin, X. J. Wu, Z. M. Luo, J. Wei, H. L. Zhang and H. Zhang, *Nanoscale*, 2014, **6**, 5624−5629.
55 S. S. Li, J. N. Zheng, X. H. Ma, Y. Y. Hu, A. J. Wang, J. R. Chen and J. J. Feng, *Nanoscale*, 2014, **6**, 5708−5713.
56 H. Nolan, N. McEvoy, M. Obrien, N. C. Berner, C. Y. Yim, T. Hallam, A. R. McDonald and G. S. Duesberg, *Nanoscale*, 2014, **6**, 8185−8191.
57 X. Sun, J. Dai, Y. Q. Guo, C. Z. Wu, F. T. Hu, J. Y. Zhao, X. C. Zeng and Y. Xie, *Nanoscale*, 2014, **6**, 8359−8367.
58 C. L. Choi, J. Feng, Y. G. Li, J. Wu, A. Zak, R. Tenne and H. J. Dai, *Nano Res*., 2013, **6**, 921−928.
59 Z. P. Huang, Z. B. Chen, Z. Z. Chen, C. C. Lv, H. Meng and C. Zhang, *ACS Nano*, 2014, **8**, 8121−8129.
60 B. E. Conway and B. V. Tilak, *Electrochim. Acta*, 2002, **47**, 3571−3594.
61 J. P. Shi, D. L. Ma, G. F. Han, Y. Zhang, Q. Q. Ji, T. Gao, J. Y. Sun, X. J. Song, C. Li, Y. S. Zhang, X. Y. Lang, Y. F. Zhang and Z. F. Liu, *ACS Nano*, 2014, **8**, 10196−10204.
62 C. Tsai, F. Abild-Pedersen and J. K. Norskov, *Nano Lett.*, 2014, **14**, 1381−1387.

Table of Contents Entry

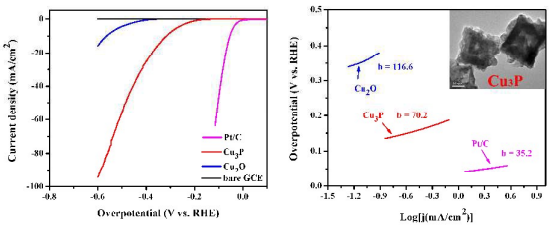

A novel Cu_3P product with excellent electrocatalytic activity toward HER was prepared through an efficient two-step strategy.